

RESEARCH ARTICLE

Three-Dimensional Turbo-Spin-Echo Amide Proton Transfer MR Imaging at 3-Tesla and Its Application to High-Grade Human Brain Tumors

Xuna Zhao,¹ Zhibo Wen,² Ge Zhang,² Fanheng Huang,² Shilong Lu,² Xianlong Wang,² Shuguang Hu,³ Min Chen,⁴ Jinyuan Zhou^{5,6}

¹Philips Healthcare, Beijing, China

²Department of Radiology, Zhujiang Hospital, Southern Medical University, Guangzhou, Guangdong, China

³Shenzhen Anke High-Tech, Shenzhen, Guangdong, China

⁴Department of Radiology, Beijing Hospital, Beijing, China

⁵Division of MR Research, Department of Radiology, Johns Hopkins University, Baltimore, MD 21287, USA

⁶F.M. Kirby Research Center for Functional Brain Imaging, Kennedy Krieger Institute, Baltimore, MD, USA

Abstract

Purpose: Amide proton transfer (APT) imaging is able to extend the achievable magnetic resonance imaging (MRI) contrast to the protein level. In this study, we demonstrate the feasibility of applying a turbo-spin-echo (TSE)-based, three-dimensional (3D) APT sequence into routine clinical practice for patients with brain tumors.

Procedures: Experiments were performed on a Philips 3-Tesla (3-T) MRI scanner using an eight-channel phased-array coil for reception. A fast 3D APT sequence with a TSE acquisition was proposed (saturation power, 2 μ T; saturation time, 500 ms; 8 slices). The gradient echo (GRE)-based field-mapping technique or water-saturation-shift-referencing (WASSR) technique was used to acquire B_0 maps to correct for B_0 -induced artifacts in APT images. The test was performed on a box of homogenous protein solution, four healthy volunteers, and eight patients with high-grade gliomas.

Results: The experimental data from a homogenous, protein-containing phantom and healthy volunteers show that the sequence produced a uniform contrast across all slices. The average $MTR_{asym}(3.5 \text{ ppm})$ values with GRE B_0 -corrected 3D APT imaging and WASSR-corrected 3D APT imaging were both comparable to the values obtained using the undemanding single-slice acquisition. The average APT image intensity was consistently higher in the tumor core than in the peripheral edema and in the contralateral normal-appearing white matter (both $P < 0.001$).

Conclusion: 3D APT imaging of brain tumors can be performed in about 5 min at 3-T using a routine, commercial eight-channel SENSE coil.

Key words: APT imaging, CEST imaging, 3D, Brain tumor, Protein, MRI

Introduction

Proteins are the most essential parts of organisms and perform almost all cellular activities. However, these

molecules cannot be detected directly by magnetic resonance (MR) imaging due to the low concentration or because of limited motion in tissue. The amide protons of mobile proteins, such as those in the cytoplasm, resonate at 8.3 ppm of the proton MR spectrum [1], namely, 3.5 ppm downfield of the water signal. There is an exchange between the amide protons of mobile proteins and the protons of bulk water, and the exchange rate is 20–30 Hz *in vivo* [2], which is

favorable for MR detection. Chemical exchange-dependent saturation transfer (CEST) imaging [3–7], a type of well-known magnetization transfer (MT) imaging [8], provides the possibility to spatially assess these mobile proteins *in vivo*, indirectly. Technically, these amide protons are selectively saturated, and the saturation is then transferred to the water protons. This process repeats itself and finally decreases the water signal intensity significantly. Because of the sensitivity enhancement with CEST, endogenous mobile proteins [9] can be assessed indirectly via the water signal. This technique is called amide proton transfer (APT) imaging [2, 10, 11].

APT imaging has been successfully applied to brain tumor [12–14] and stroke [15] patients at 3-Tesla (3-T), but these clinical applications are mainly limited to a single-slice acquisition, due to several technical limitations, such as high radiofrequency (RF) power deposition and the long scan time required for multiple acquisitions at different frequencies. Recently, several volumetric APT imaging techniques were proposed [16–21]. For example, Sun *et al.* [16] reported a multi-slice APT imaging technique in an animal system. This technique obtained a five-slice acquisition after the completion of a single long RF irradiation and then compensated the relaxation loss between earlier and later slices with the post-processing method. Dixon *et al.* [17] reported another multi-slice gradient-echo CEST imaging method at 1.5-T. The sequence was composed of several interleaved, short pre-saturation pulses and spatially selective observation pulses, and five slices were acquired. Notably, Zhu *et al.* [18] developed a fast, three-dimensional (3D) whole-brain CEST technique at 3-T. The sequence used a gradient- and spin-echo (GRASE) readout, with an asymmetric frequency-modulated pulse to suppress the lipid signal and a 32-channel phased-array coil to achieve a sensitivity-encoding (SENSE) acceleration factor of four. Jones *et al.* [21] reported another fast, 3D whole-brain, steady-state CEST sequence at 7-T. The sequence consisted of numerous brief saturation pulses, each followed by a segmented echo-planar imaging (EPI) acquisition. Compared with the multi-slice imaging, the 3D acquisition is preferred for volume APT imaging because of its minimized relaxation loss between slices, large volume coverage, high signal-to-noise ratio, and reasonable acquisition time [18].

In this study, we present a 3D APT imaging sequence using the turbo-spin-echo (TSE) acquisition that is based on the routine eight-channel SENSE coil. Clinical applications are demonstrated through the imaging of brain tumors.

Materials and Methods

Phantoms and Human Subjects

In phantom experiments, a box of homogenous bovine serum albumin (BSA) solution (10 % protein concentration) was used. In human studies, four healthy volunteers (three males, one female;

age range, 20–46 years; mean, 34.2 years) and eight patients (six males, two females; age range, 7–55 years; mean, 29.6 years; see Table 1 for patient information in more detail) with high-grade brain tumors were investigated. The study protocol was approved by the local Institutional Review Board. All volunteers and patients provided written, informed consent.

MRI Protocol

Experiments were performed on a Philips 3-T magnetic resonance imaging (MRI) scanner (Achieva 3.0-T; Philips Healthcare Systems, Best, The Netherlands) equipped with a pencil-beam, second-order shim, using a body coil for RF transmission and an eight-channel SENSE coil for reception.

In the 3D APT imaging experiments, an off-resonance long RF saturation pulse with a duration of 500 ms (which is the longest allowed for our body coil) and a power level of 2 μT (which was optimized in our recent study [15]) was used. Multiple frequency offsets (M_0 , ± 3 , ± 3.5 [2], and ± 4 ppm; the values in brackets were the number of acquisitions, which was 1, if not specified) were acquired. Other imaging parameters for 3D volumetric APT imaging were: TSE readout; TSE factor=54; SENSE factor=1.7; repetition time (TR)=2,500 ms; echo time (TE)=11 ms; matrix=128 \times 64; field of view=240 \times 240 mm²; 8 slices or points; thickness or resolution=6.0 mm; scan time=5.3 min. Two B_0 field-mapping methods were used for comparison. One was the gradient echo (GRE)-based field-mapping method, and the other was the so-called water-saturation-shift-referencing method (WASSR) [22]. For the former, a 3D T_1 fast-field-echo sequence was used (TR=30 ms). Five phase images, with TEs of 1.28, 2.28, 3.28, 4.28, and 5.28 ms, were acquired to obtain a B_0 map. For the latter, an RF saturation sequence with a low B_1 (0.2 μT) and a short time (100 ms) was used, and the data were acquired with a multi-offset scheme (0, ± 12 , ± 24 , ± 36 , ± 48 , ± 60 , ± 72 , ± 84 , ± 96 , and ± 108 Hz; 1 ppm=128 Hz at 3-T). These two B_0 field methods took 23 s and 1.7 min, respectively. To ensure the same B_0 fields for the B_0 scans and APT scans, the f_0 determination and shimming functions were turned off during the prescan of the field-mapping acquisitions (after the APT image data were acquired). The specific absorption rate (SAR) was 2.7 W/kg for the 3D APT imaging scan; 1.0 W/kg for the GRE B_0 scan; and 0.3 W/kg for the WASSR B_0 scan; all of which were within the FDA guidelines (3 W/kg averaged over the head for any 10-min period).

Single-slice APT imaging was acquired for comparison. The single-slice acquisition protocol proposed previously [14] was used, in which the APT image scan and z-spectrum scan were combined (31 offsets=0, ± 0.25 , ± 0.5 , ± 0.75 , ± 1 , ± 1.5 , ± 2 , ± 2.5 , ± 3 [2], ± 3.25 [4], ± 3.5 [8], ± 3.75 [4], ± 4 [2], ± 4.5 , ± 5 , and ± 6 ppm; an unsaturated image was acquired for the signal normalization). Other single-slice imaging parameters were: single-shot TSE readout; TSE factor=42; SENSE factor=1.7; TR=2,500 ms; TE=11 ms; matrix=128 \times 64; field of view=240 \times 240 mm²; scan time=2.7 min; and SAR=1.3 W/kg.

For reference, several standard MR images, including T_2 -weighted, T_1 -weighted, fluid-attenuated inversion recovery (FLAIR), and gadolinium (Gd)-enhanced T_1 -weighted, were acquired. The parameters used were: T_2 -weighted (TSE factor=8, TR/TE=3,000/80 ms, 18 slices, thickness=6.0 mm, sense factor=1.6); T_1 -weighted (3D magnetization-prepared-rapid-gradient-echo sequence, TR/TE/TI=2,000/20/800 ms, 18 slices, thickness=6.0 mm,

Table 1. Patient characteristics and pathology results

No.	Age	Sex	Lesion location	Clinical presentation	Pathology
1	38	M	Right temporal–parietal	Headache	Glioblastoma multiforme
2	16	M	Left temporal	Dizziness and seeing double	Glioblastoma multiforme
3	26	M	Right parietal	Dizziness and seizure	Astrocytoma, grade III
4	15	M	Left temporal	Headache and nausea	Ependymoma, grade III
5	55	M	Right basal ganglia	Weakness of left limb	Astrocytoma, grade III
6	55	F	Right temporal	Headache	Glioblastoma multiforme
7	25	F	Right temporal	Convulsion and coma	Astrocytoma, grade III
8	7	M	Left frontal–parietal	Weakness of left limb	Glioblastoma multiforme

SENSE factor=1.6); FLAIR (TSE factor=27, TR/TE/TI=11,000/125/2,800 ms, 18 slices, sense factor=1.6); and Gd-enhanced T₁-weighted (single-shot turbo field echo, flip angle=15°, TR/TE=15/4.6 ms, thickness=6.0 mm, SENSE factor=1.6). The APT images were acquired before the administration of the Gd contrast agent.

Theory

The APT effect reflects the cellular protein information in the biological tissue but contains the concurrent saturation effects, such as conventional MT and direct water saturation. The MT ratio (MTR) is defined as $1 - S_{\text{sat}}/S_0$, where S_{sat} and S_0 are the signal intensities with and without selective irradiation, respectively. In order to remove these unwanted contributions, the asymmetry analysis of MTR with respect to the water frequency is generally used:

$$\begin{aligned} \text{MTR}_{\text{asym}}(\text{offset}) &= \text{MTR}(+\text{offset}) - \text{MTR}(-\text{offset}) \\ &= S_{\text{sat}}(-\text{offset})/S_0 - S_{\text{sat}}(+\text{offset})/S_0. \end{aligned} \quad (1)$$

For APT imaging, the asymmetry analysis at 3.5 ppm downfield from the water signal is calculated as [2, 10, 11]:

$$\begin{aligned} \text{MTR}_{\text{asym}}(3.5\text{ppm}) &= S_{\text{sat}}(-3.5\text{ppm})/S_0 - S_{\text{sat}}(3.5\text{ppm})/S_0 \\ S_0 &\approx \text{MTR}'_{\text{asym}}(3.5\text{ppm}) + \text{APTR}, \end{aligned} \quad (2)$$

where $\text{MTR}'_{\text{asym}}(3.5\text{ ppm})$ is the inherent asymmetry of the conventional MT effect associated with immobile macromolecules and membranes (which is usually negative) [23], and APTR is the proton transfer ratio for the amide protons. Although the asymmetry analysis was performed, a small, residual MTR asymmetry still exists. This is because the conventional MT effect is not absolutely symmetric with respect to water *in vivo*, which contributes a negative background signal. Thus, the measured $\text{MTR}_{\text{asym}}(3.5\text{ ppm})$ is just an apparent APT signal, and the calculated $\text{MTR}_{\text{asym}}(3.5\text{ ppm})$ images should be called APT-weighted images and APT images (for simplicity).

The APT images were susceptible to B₀ inhomogeneity, although the pencil-beam shimming was employed, and these images have to be corrected according to the B₀ field information. Three APT images with the different B₀ corrections were compared in this study: single-slice APT; GRE B₀-corrected 3D APT; and WASSR-corrected 3D APT.

Data Analysis

All data processing procedures were performed using the interactive data language (IDL, version 7; Exelis Visual Information Solutions, Inc., Boulder, CO). For the single-slice APT imaging, a full z-spectrum (S_{sat}/S_0 as a function of frequency offset relative to water) was fitted through 31 offsets using a 12th-order polynomial (the maximum order available with IDL) on a voxel-by-voxel basis. The fitted curve was interpolated using an offset resolution of 1 Hz. The corresponding B₀ field inhomogeneity was calculated according to the deviation of the minimum of the fitted curve from 0 ppm, and the measured z-spectrum for each voxel was shifted along the direction of the offset axis accordingly. Then, the realigned z-spectra were interpolated back to 31 points, and the $\text{MTR}_{\text{asym}}(3.5\text{ ppm})$ image was calculated.

The 3D APT data were processed with two different methods. For the GRE B₀-corrected 3D APT images, the B₀ map was first fitted from the five phase images (TE=1.28, 2.28, 3.28, 4.28, and 5.28 ms). For the WASSR-corrected 3D APT images, a z-spectrum, dominated by direct water saturation, was fitted through 19 offsets, using a 12th-order polynomial on a voxel-by-voxel basis. The fitted curve was interpolated using an offset resolution of 1 Hz. The water center frequency in each voxel was determined by the minimum of the fitted curve from 0 ppm accordingly. Then, to correct for the field inhomogeneity effects in the APT images, the acquired APT data at offsets (+4, +3.5, +3 ppm) for each voxel were interpolated to 257 points, over a range from +4.5 to +2.5 ppm (1 Hz resolution), and shifted using the B₀ value for the same voxel. A similar procedure was applied to the negative-offset data (−3, −3.5, −4 ppm). Finally, the corrected APT images with two different B₀ maps, the GRE B₀-corrected 3D APT images and the WASSR-corrected 3D APT images, were calculated using the shift-corrected data at ±3.5 ppm. All APT images were thresholded, based on the signal intensity of the S₀ image, to remove voxels outside the brain.

For the quantitative analysis, regions of interest were chosen by two experienced radiologists (ZW and XW, who had ~20 and 10 years of experience in brain tumor imaging, respectively). For normal brain tissues, regions of interest were drawn on relatively homogenous white matter. For brain tumors, the regions of interest were placed according to the signal abnormalities on the Gd-enhanced, T₁-weighted and other MR images, with the support of the histopathological findings. The contralateral normal-appearing white matter was also chosen for reference. All results were expressed as mean±standard deviation. A one-way analysis of variance test, followed by multiple comparisons

of the Tukey's test, was used to evaluate the statistics, using the statistical package SPSS for Windows (version 18, Chicago, IL). Differences were considered statistically significant if $P < 0.05$.

Results

Single-Slice and 3D APT Experiments on a Phantom

Fig. 1 shows the z-spectrum and $MTR_{\text{asym}}(3.5 \text{ ppm})$ results acquired using the 3D TSE APT imaging sequence and the single-slice APT imaging sequence (repeated single-slice APT) on a phantom of homogeneous BSA solution with a 10 % protein concentration. The experimental data show that the average $MTR_{\text{asym}}(3.5 \text{ ppm})$ values across eight slices for both GRE B_0 -corrected 3D APT imaging and WASSR-corrected 3D APT imaging were comparable with those of repeated single-slice APT imaging. In addition, for GRE B_0 -corrected 3D APT and WASSR-corrected 3D APT, the average $MTR_{\text{asym}}(3.5 \text{ ppm})$ values did not vary obviously, and there was no visual signal loss due to T_1 relaxation in 3D acquisition across slices, as expected.

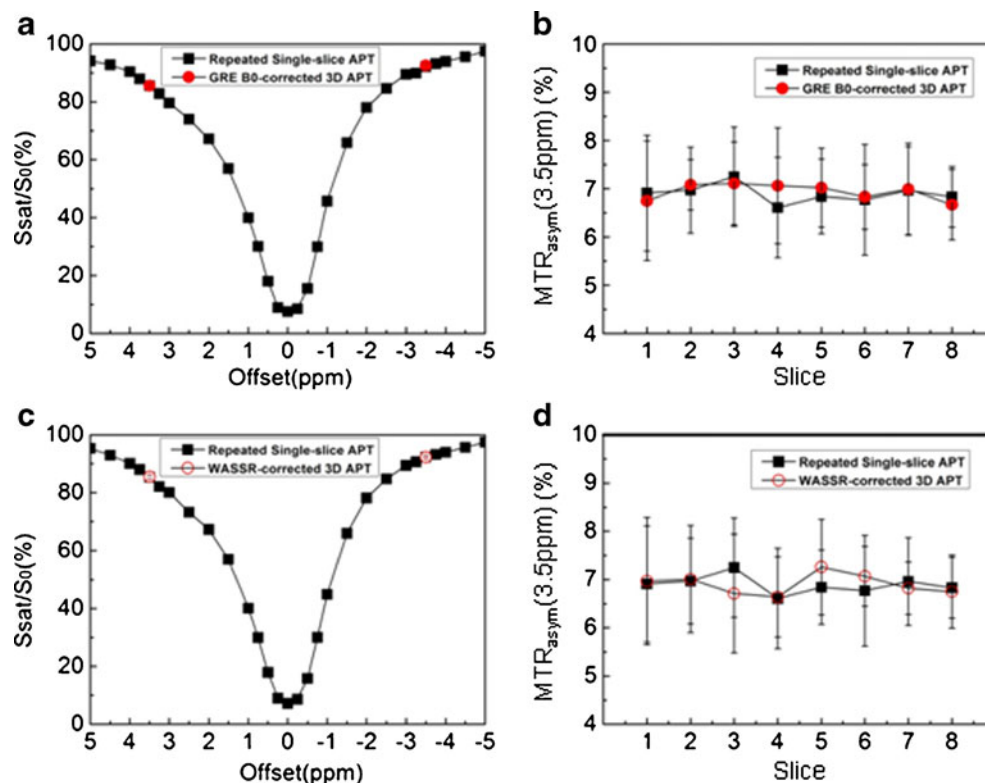


Fig. 1. Z-spectra and $MTR_{\text{asym}}(3.5 \text{ ppm})$ values measured by single-slice and 3D APT imaging on a homogenous BSA solution. The single-slice experiment was repeated eight times to cover all slices. **a, b** Single-slice APT versus GRE B_0 -corrected 3D APT. **c, d** Single-slice APT versus WASSR-corrected 3D APT. The error bars in z-spectra were too small to see clearly. Volumetric APT imaging z-spectra and $MTR_{\text{asym}}(3.5 \text{ ppm})$ results were similar to single-slice results and were uniform across the slices.

Single-Slice and 3D APT Experiments on Normal Subjects

Fig. 2 shows the T_2 -weighted image, B_0 maps from the single-slice APT, multiple GRE and WASSR scans, and the $MTR_{\text{asym}}(3.5 \text{ ppm})$ image without the B_0 inhomogeneity correction. Also displayed in Fig. 2 are the $MTR_{\text{asym}}(3.5 \text{ ppm})$ images using the single-slice technique, the GRE B_0 -corrected 3D APT approach, and the WASSR-corrected 3D APT approach, all of which were obtained from a typical normal subject. Although the higher-order shimming was employed, the serious magnetic field inhomogeneity-related artifacts were still seen in the acquired (uncorrected) APT image (Fig. 2e). The appropriate B_0 field inhomogeneity corrections were required. For the 3D APT imaging, we acquired two B_0 field maps (Fig. 2c, d) under the same shimming conditions as the 3D APT imaging scan. The B_0 field inhomogeneity as seen in the maps was typically less than 20 Hz in the relevant brain regions but could be more than 100 Hz near air-tissue interfaces (sinus, ear). The variation between these two B_0 maps was less than 5 Hz in most brain areas. In the corrected $MTR_{\text{asym}}(3.5 \text{ ppm})$ images, including the single-slice APT, the GRE B_0 -corrected 3D APT, and the WASSR-corrected 3D APT, the artifacts that resulted

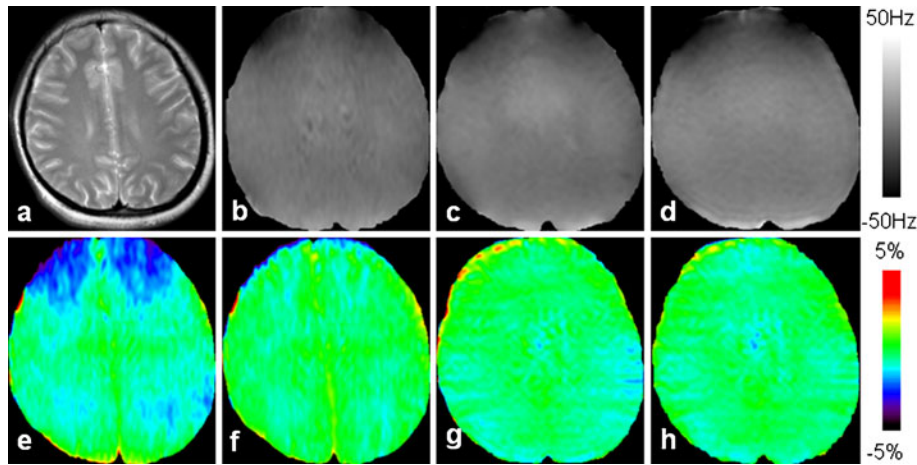


Fig. 2. **a** T₂-weighted image from a healthy volunteer. **b–d** B₀ maps from the single-slice APT, GRE, and WASSR experiments. **e** Single-slice APT images without B₀ inhomogeneity correction. **f–h** Corrected single-slice APT image, GRE B₀-corrected 3D APT image, and WASSR-corrected 3D APT image.

from the B₀ field inhomogeneity were virtually absent, and the APT images were homogenous in most brain regions.

Fig. 3 compares the MTR_{asym}(3.5 ppm) results for single-slice APT, GRE B₀-corrected 3D APT, and WASSR-corrected

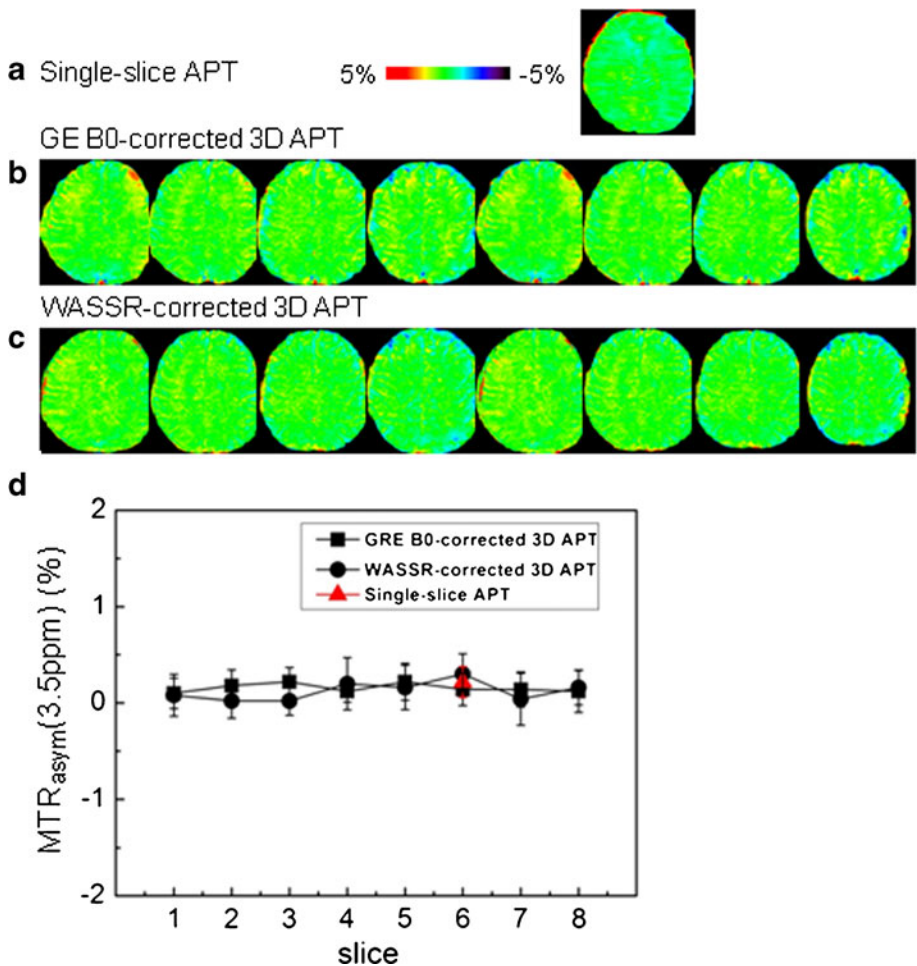


Fig. 3. **a–c** Corrected single-slice APT image, GRE B₀-corrected 3D APT image, and WASSR-corrected 3D APT image from a healthy human subject. **d** Measured MTR_{asym}(3.5 ppm) values with the single-slice APT sequence and 3D sequence (GRE B₀-corrected and WASSR-corrected) (n=4). The position of the single-slice acquisition corresponded to the position of slice 6 from the 3D sequence. The measured values for the two 3D protocols were uniform across the slices, and both were very close to that of the single-slice APT image for the corresponding slice.

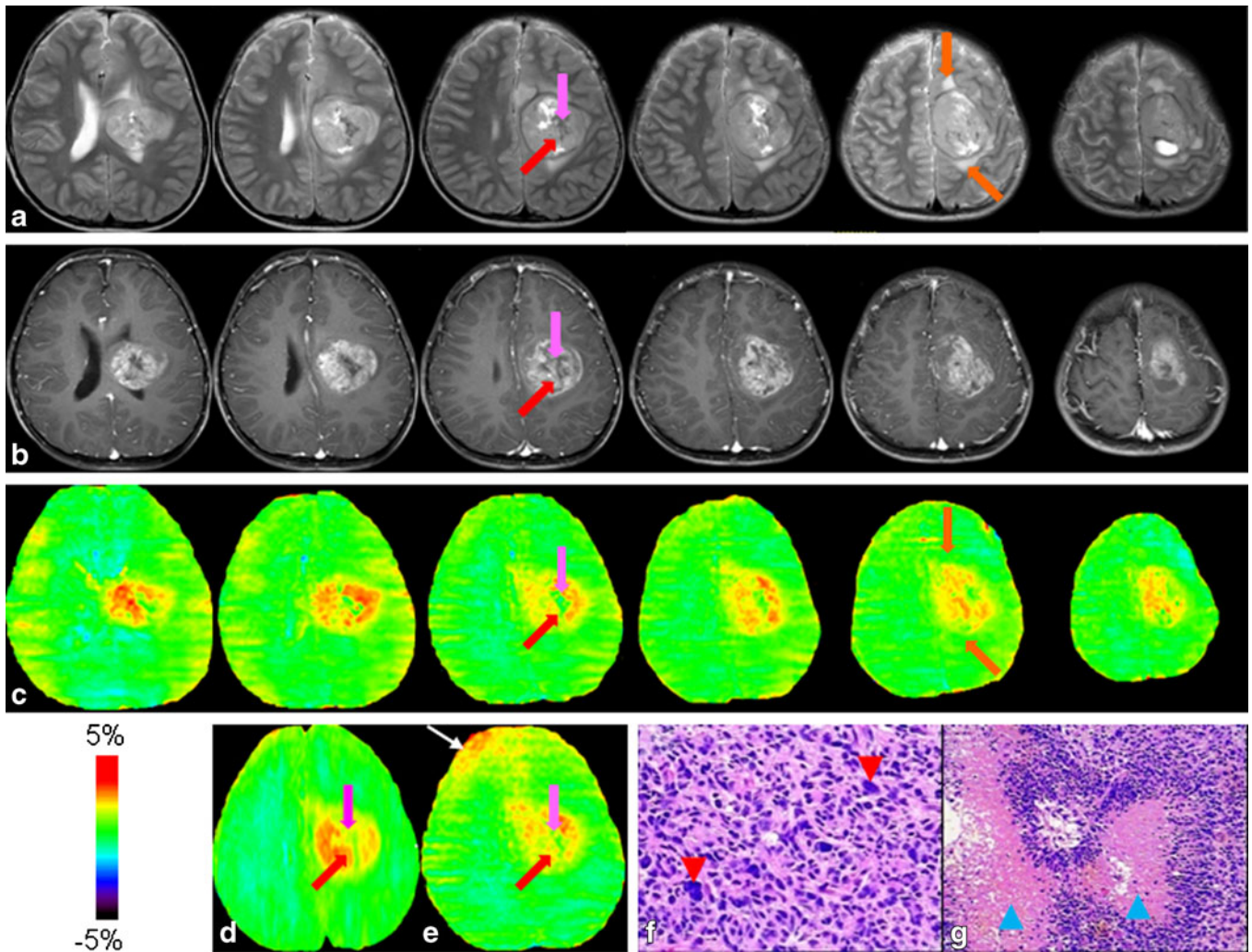


Fig. 4. MR images for a patient (patient 8) with glioblastoma. **a** T_2 -weighted images show a heterogeneous tumor mass. **b** Gd-enhanced, T_1 -weighted images demonstrate heterogeneous enhancement (*red arrow*) with some non-enhancing necrotic areas (*pink arrow*). **c** APT images (WASSR-corrected) show that the Gd-enhancing tumor core is hyperintense, while the necrotic region and the surrounding edematous area (*orange arrow*) are both hypointense. **d** Single-slice APT image corresponding to the third slice of (c). **e** GRE B_0 -corrected 3D APT image corresponding to the third slice of (c). **f, g** Histopathological sections sampled from the tumor core and necrotic area, respectively. *Red arrowhead*: irregular tumor cells; *blue arrowhead*: “false fence” necrosis.

3D APT methods from healthy volunteers ($n=4$). The single-slice acquisition was localized at slice 6 from the 3D sequence. For both GRE B_0 -corrected 3D APT and WASSR-corrected 3D APT, the $MTR_{\text{asym}}(3.5 \text{ ppm})$ images show relative homogeneity in all slices, and no large B_0 field inhomogeneity artifacts were seen. The measured average $MTR_{\text{asym}}(3.5 \text{ ppm})$ data from both 3D approaches were nearly constant across all slices. For slice 6, the measured $MTR_{\text{asym}}(3.5 \text{ ppm})$ from GRE B_0 -corrected 3D APT and WASSR-corrected 3D APT images was $0.14\% \pm 0.18\%$ and $0.30\% \pm 0.21\%$, respectively, which were very close to the single-slice APT value ($0.22\% \pm 0.16\%$). Note that the measured $MTR_{\text{asym}}(3.5 \text{ ppm})$ values were almost zero, because the $MTR'_{\text{asym}}(3.5 \text{ ppm})$ (which is negative) and APTR (which is positive) nearly canceled each other out at $2 \mu\text{T}$, as reported in our previous study [15].

Single-Slice and 3D APT Experiments on Patients with High-Grade Brain Tumors

Fig. 4 shows an example of APT images for a patient (patient 8), who had a pathologically proven high-grade glioma (size, $5.1 \times 4.4 \times 6.2 \text{ cm}^3$) in the left frontal–parietal lobe. The tumor core, as identified by the signal enhancement in the post-contrast T_1 -weighted images (Fig. 4b), was consistent with the area of hyperintensity in the APT images (Fig. 4c). The APT hyperintensity (compared with the contralateral white matter) is a typical feature of high-grade (grade III and IV) brain tumors, in line with expectations based on the increased content of cellular proteins in lesions. The surrounding peritumoral edema that was hyperintense on T_2 -weighted images exhibited isointensity (relative to the contralateral normal-appearing white matter) on the APT images. For the same slice, the

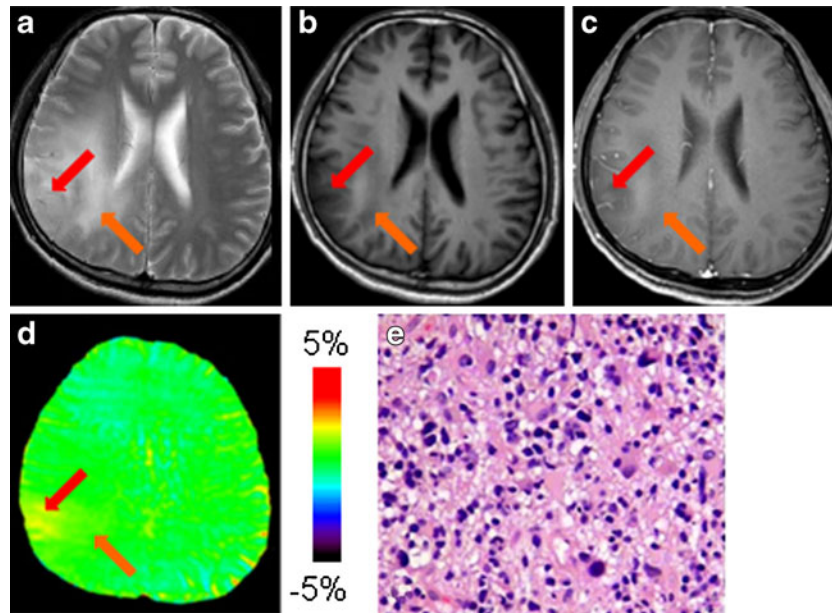


Fig. 5. MR images for a patient (patient 3) with a grade-III astrocytoma. **a** T₂-weighted image. **b** T₁-weighted images before Gd injection. **c** Gd-enhanced T₁-weighted image. **d** GRE-corrected APT image identifies a portion of high APT signal intensity (tumor core; red arrow) and a large APT-isointense peritumoral edematous area (orange arrow). **e** Histopathological section confirms the existence of high-density tumor cells in the tumor core.

tumor appearance on the GRE B₀-corrected APT image or on the WASSR-corrected APT image was comparable to the appearance on the single-slice APT image. The specimens were sampled from the tumor core and necrotic areas, respectively. The tumor core showed histopathological characteristics with abundant irregular tumor cells (Fig. 4f) and “false fence” necrosis (Fig. 4g).

Fig. 5 shows the standard and APT images from a patient with a grade-III astrocytoma (patient 3) in the right parietal lobe. In this case, there is no obvious signal enhancement in the Gd-enhanced T₁-weighted image. However, the markedly elevated APT signal intensity is still visible within the T₂-hyperintense lesion. The region with high APT signal was sampled during the clinical surgical procedure. The histopathological exam shows high tumor cellularity, no necrosis, and little vascular proliferation. The result confirms the radiological diagnosis of grade-III astrocytoma. This case illustrates that APT images can provide additional information about the presence and grade of brain tumors, especially when Gd enhancement is not available.

Table 2 shows the MTR_{asym}(3.5 ppm) values for the same slice measured with three different B₀ correction methods, single-slice APT, GRE B₀-corrected 3D APT, and WASSR-corrected 3D APT. For the tumor core, peritumoral edema, or contralateral brain tissue, the measured MTR_{asym}(3.5 ppm) values were comparable, and there were no significant differences between the values for the different methods ($P > 0.2$). For all gliomas, the average MTR_{asym}(3.5 ppm) values were significantly higher in the tumor core than in the peritumoral edema and in the contralateral brain tissue (both $P < 0.001$).

Discussion

APT imaging is a novel molecular MRI method and has drawn considerable attention recently [24–29]. However, several issues must be considered to obtain a good APT contrast. First, to maximize the APT signal for the low-concentration (micromolar to millimolar) cellular mobile proteins, a long, low-power RF irradiation pulse or an RF pulse-train scheme is required. Second, a sufficient signal-to-noise ratio is always required, which may require multiple acquisitions for averaging. Third, according to the RF radiation power dependence properties of the APT signal, an appropriate RF irradiation power should be selected. Last, but not least, some attention should be paid to the B₀ inhomogeneity that may cause a significant artifact in APT images. Thus, it is necessary to develop some methods to correct for local frequency shifts. When APT imaging was translated to the clinic, more problems have to be solved, such as the large volume coverage, feasible scan times, permissible RF power deposition, *etc.* Recently, several high-quality clinical results from the application of APT imaging have been reported [14, 15]. However, these clinical studies were mainly restricted to a single-slice acquisition, as the acquisition schemes acquired a full z-spectrum with about 30 frequency offsets and were time-consuming.

To improve the clinical significance, volumetric APT imaging should be developed. Technically, it would be desirable to design a 3D APT imaging sequence that provides enough imaging coverage as well as good contrast. Moreover, this 3D APT acquisition should not require a long scan time to avoid possible motion artifacts. Practically, it is

Table 2. Measured $MTR_{\text{asym}}(3.5 \text{ ppm})$ values for brain tumors ($n=8$) with single-slice APT, GRE B_0 -corrected 3D APT, and WASSR-corrected 3D APT

		Tumor core	Peritumoral edema	Contralateral
Single-slice APT	Mean \pm SD	2.4 \pm 0.3	0.4 \pm 0.2	0.2 \pm 0.2
	Value range	(2.0, 2.8)	(0.1, 0.6)	(-0.3, 0.4)
GRE B_0 -corrected 3D APT	Mean \pm SD	2.4 \pm 0.3	0.5 \pm 0.3	0.2 \pm 0.2
	Value range	(2.0, 2.8)	(0.1, 1.2)	(-0.1, 0.5)
WASSR-corrected 3D APT	Mean \pm SD	2.3 \pm 0.2	0.5 \pm 0.3	0.1 \pm 0.1
	Value range	(2.0, 2.6)	(0.1, 0.8)	(-0.1, 0.4)

better than a routine MRI coil, such as the eight-channel SENSE coil, should be used, which will help to extend the clinical application of the APT technique. In the proton MR spectrum, the lipid protons resonate at 1.3 ppm, and the amide protons appear at around 8.3 ppm. Their chemical shift differences from water (4.7 ppm) are almost the same, but of opposite sign. This would lead to the extra saturation of lipid protons in the reference scan [$S_{\text{sat}}(-3.5 \text{ ppm})$], but not in the APT scan [$S_{\text{sat}}(3.5 \text{ ppm})$], thus incurring a lipid artifact when the asymmetry analysis is used. To hasten the 3D acquisition, a rapid acquisition technique, such as EPI, TSE, or GRASE, is preferred. Our experience shows that EPI or GRASE may bring about more serious lipid artifacts [18], compared with the TSE acquisition, especially when a 32-channel phased-array coil is used. The TSE sequence was used for the 3D APT acquisition in this study because of its high image quality and fewer lipid artifacts. Although the TSE acquisition suffered from a relatively high SAR, our experimental results showed that the SAR was still within the FDA limitations.

The B_0 field inhomogeneity maps can be obtained quickly by the GRE-based field-mapping and the WASSR methods [22]. Based on these, we proposed two 3D volumetric APT imaging schemes (GRE B_0 -corrected 3D APT and WASSR-corrected 3D APT) that can be used in any standard clinical 3-T setting. Notably, the APT imaging scan time is only about 5 min. Such fast volumetric APT imaging techniques should be particularly useful in the clinic. In this work, we paid more attention to the feasibility analysis of these fast 3D schemes. In the phantom and normal volunteer studies, we found that the measured $MTR_{\text{asym}}(3.5 \text{ ppm})$ value for each slice using the 3D APT acquisitions was comparable to the value for the corresponding slice using the single-slice APT acquisition. Moreover, these values do not vary across the slices obviously. The results demonstrated that both 3D APT experimental schemes can offer experimental results similar to those of the single-slice APT scheme. In addition, both 3D APT schemes can remove most artifacts caused by the B_0 inhomogeneity, just as the single-slice APT did. Quantitatively, the $MTR_{\text{asym}}(3.5 \text{ ppm})$ values in several regions were compared for the three experimental methods (Table 2). The results show that these three B_0 correction methods gave comparable $MTR_{\text{asym}}(3.5 \text{ ppm})$ results.

Our 3D APT acquisition schemes can provide good clinical experimental results for brain tumors and do not require any special hardware or software but can offer more

information about lesions. Just as with our previous single-slice-based experimental results [12–14], the addition of 3D APT imaging to the standard MRI protocol may help distinguish the heterogeneity of a malignant brain tumor, and these capabilities of APT imaging may be very important in the diagnosis and treatment planning for patients with brain tumors.

Conclusions

We have developed and validated a 3D APT imaging experimental scheme, at 3-T, that uses a standard, commercial eight-channel SENSE coil for reception. The technique uses the GRE field-mapping method or the WASSR method to obtain B_0 -corrected 3D volumetric APT images in about 5 min. Our experimental results showed that this 3D APT sequence with the TSE acquisition can provide good image quality and enough volume coverage for clinical applications, such as for the imaging of brain tumors. The early results suggest that 3D APT may be a valuable addition to the MRI armamentarium for the accurate characterization of human brain tumors.

Acknowledgments. This work was supported in part by grants from the National Institutes of Health (R01EB009731, R01EB015032, R21EB009112, R21EB015555, and P41EB015909), the National Natural Science Foundation of China (81128006 and 81171322), and Dana Foundation. We thank Ms. Mary McAllister for editorial assistance.

Conflict of Interest. J.Z. is a co-inventor on a patent at the US Patent and Trademark Office for the APT-MRI technology. This patent is owned and managed by Johns Hopkins University.

References

1. Wuthrich K (1986) NMR of proteins and nucleic acids, 2nd edn. John Wiley & Sons, New York
2. Zhou J, Payen J, Wilson DA, Traystman RJ, van Zijl PC (2003) Using the amide proton signals of intracellular proteins and peptides to detect pH effects in MRI. *Nature Med* 9:1085–1090
3. Ward KM, Aletras AH, Balaban RS (2000) A new class of contrast agents for MRI based on proton chemical exchange dependent saturation transfer (CEST). *J Magn Reson* 143:79–87
4. Zhou J, van Zijl PC (2006) Chemical exchange saturation transfer imaging and spectroscopy. *Progr NMR Spectr* 48:109–136
5. Aime S, Crich SG, Gianolio E, Giovenzana GB, Tei L, Terreno E (2006) High sensitivity lanthanide(III) based probes for MR-medical imaging. *Coord Chem Rev* 250:1562–1579
6. Sherry AD, Woods M (2008) Chemical exchange saturation transfer contrast agents for magnetic resonance imaging. *Annu Rev Biomed Eng* 10:391–411
7. Hancu I, Dixon WT, Woods M, Vinogradov E, Sherry AD, Lenkinski RE (2010) CEST and PARACEST MR contrast agents. *Acta Radiol* 51:910–923

8. Wolff SD, Balaban RS (1989) Magnetization transfer contrast (MTC) and tissue water proton relaxation *in vivo*. *Magn Reson Med* 10:135–144
9. Zhou JY, Yan K, Zhu H (2012) A simple model for understanding the origin of the amide proton transfer MRI signal in tissue. *Appl Magn Reson* 42(3):393–402
10. Zhou J, Lal B, Wilson DA, Larterra J, van Zijl PCM (2003) Amide proton transfer (APT) contrast for imaging of brain tumors. *Magn Reson Med* 50:1120–1126
11. Zhou J, Tryggstad E, Wen Z et al (2011) Differentiation between glioma and radiation necrosis using molecular magnetic resonance imaging of endogenous proteins and peptides. *Nat Med* 17:130–134
12. Jones CK, Schlosser MJ, van Zijl PC, Pomper MG, Golay X, Zhou J (2006) Amide proton transfer imaging of human brain tumors at 3T. *Magn Reson Med* 56:585–592
13. Zhou J, Blakeley JO, Hua J et al (2008) Practical data acquisition method for human brain tumor amide proton transfer (APT) imaging. *Magn Reson Med* 60:842–849
14. Wen Z, Hu S, Huang F et al (2010) MR imaging of high-grade brain tumors using endogenous protein and peptide-based contrast. *NeuroImage* 51:616–622
15. Zhao X, Wen Z, Huang F et al (2011) Saturation power dependence of amide proton transfer image contrasts in human brain tumors and strokes at 3T. *Magn Reson Med* 66:1033–1041
16. Sun PZ, Murata Y, Lu J, Wang X, Lo EH, Sorensen AG (2008) Relaxation-compensated fast multislice amide proton transfer (APT) imaging of acute ischemic stroke. *Magn Reson Med* 59:1175–1182
17. Dixon WT, Hancu I, Ratnakar SJ, Sherry AD, Lenkinski RE, Alsop DC (2009) A multislice gradient echo pulse sequence for CEST imaging. *Magn Reson Med* 63:253–256
18. Zhu H, Jones CK, van Zijl PCM, Barker PB, Zhou J (2010) Fast 3D chemical exchange saturation transfer (CEST) imaging of the human brain. *Magn Reson Med* 64:638–644
19. Sun PZ, Cheung JS, Wang E, Berner T, Sorensen AG (2011) Fast multislice pH-weighted chemical exchange saturation transfer (CEST) MRI with unevenly segmented RF irradiation. *Magn Reson Med* 65:588–594
20. Park SH, Duong TQ (2011) Alternate ascending/descending directional navigation approach for imaging magnetization transfer asymmetry. *Magn Reson Med* 65(6):1702–1710
21. Jones CK, Polders D, Hua J, et al. (2012) *In vivo* 3D whole-brain pulsed steady state chemical exchange saturation transfer at 7T. *Magn Reson Med* 67:1579–1589
22. Kim M, Gillen J, Landman BA, Zhou J, van Zijl PCM (2009) Water saturation shift referencing (WASSR) for chemical exchange saturation transfer (CEST) experiments. *Magn Reson Med* 61:1441–1450
23. Hua J, Jones CK, Blakeley J, Smith SA, van Zijl PCM, Zhou J (2007) Quantitative description of the asymmetry in magnetization transfer effects around the water resonance in the human brain. *Magn Reson Med* 58:786–793
24. Sun PZ, Zhou J, Sun W, Huang J, van Zijl PCM (2007) Detection of the ischemic penumbra using pH-weighted MRI. *J Cereb Blood Flow Metab* 27:1129–1136
25. Jokivarsi KT, Grohn HI, Grohn OH, Kauppinen RA (2007) Proton transfer ratio, lactate, and intracellular pH in acute cerebral ischemia. *Magn Reson Med* 57:647–653
26. Mougín OE, Coxon RC, Pitiot A, Gowland PA (2010) Magnetization transfer phenomenon in the human brain at 7T. *NeuroImage* 49:272–281
27. Jia G, Abaza R, Williams JD et al (2011) Amide proton transfer MR imaging of prostate cancer: a preliminary study. *J Magn Reson Imaging* 33(3):647–654
28. Dula AN, Asche EM, Landman BA et al (2011) Development of chemical exchange saturation transfer at 7T. *Magn Reson Med* 66(3):831–838
29. Scheidegger R, Vinogradov E, Alsop DC (2011) Amide proton transfer imaging with improved robustness to magnetic field inhomogeneity and magnetization transfer asymmetry using saturation with frequency alternating RF irradiation. *Magn Reson Med* 66(5):1275–1285